Proc. Natl. Acad. Sci. USA
Vol. 95, pp. 8692–8697, July 1998
Genetics

Targeted disruption of *Pax1* defines its null phenotype and proves haploinsufficiency

BETTINA WILM, EDGAR DAHL*, HEIKO PETERS, RUDI BALLING, AND KENJI IMAI†

GSF-National Research Center for Environment and Health, Institute of Mammalian Genetics, 85764 Neuherberg, Germany

Edited by Mary F. Lyon, Medical Research Council, Oxon, United Kingdom, and approved May 28, 1998 (received for review April 6, 1998)

ABSTRACT **The murine paired box-containing gene *Pax1* is required for normal development of the vertebral column, the sternum, and the scapula. Previous studies have shown that three natural *Pax1* mouse mutants, the *undulated* alleles, exhibit phenotypes of different severity in these skeletal elements. Nevertheless, these analyses have not clarified whether the semidominant *Undulated short-tail* (*Un^s*) mutation, in which the complete *Pax1* locus is deleted, represents a null allele. Moreover, the analyses of the classical *undulated* mutants did not allow a conclusion with respect to haploinsufficiency of *Pax1*. To address both questions we have created a *Pax1* null allele in mice by gene targeting. Surprisingly, the phenotype of this defined mutation exhibits clear differences to that of *Un^s*. This result strongly indicates the contribution of additional gene(s) to the *Un^s* mutant phenotype. Furthermore, the phenotype of mice heterozygous for the null allele demonstrates that *Pax1* is haploinsufficient in some though not all skeletal elements which express *Pax1* during embryonic development.**

In vertebrates the paired box-containing (*Pax*) genes consist of nine members (*Pax1–Pax9*) that code for a family of transcription factors (1, 2). The common motif shared by Pax proteins is the paired domain, which consists of 128 amino acids (3) and exerts the DNA binding function (4). The characterization and analysis of mutations affecting *Pax* genes in mice, humans, and other species have elucidated their important roles in a variety of tissues during embryonic development (5–8).

In the mouse, expression of *Pax1* can be detected in sclerotomal cells from embryonic day 8.5 (E8.5) onward (9, 10). As development proceeds, *Pax1* transcripts become confined to mesenchymal condensations, which represent the anlagen of the intervertebral discs, and to the perichondria surrounding the cartilage blastemas of the vertebral bodies (10). *Pax1* expression starts also in the pharyngeal pouches at E9.5 (11), in the anterior proximal region of the limb buds at E10.0 (12), and in the developing sternum at E13.0 (ref. 9; E.D. and K.I., unpublished observation).

The three classical *undulated* alleles in the mouse (13–15) harbor mutations of the *Pax1* gene (16, 17). In *undulated* (*un*), an amino acid exchange at a conserved position of the paired domain of Pax1 causes reduced DNA binding affinity and altered specificity of the mutant protein (16, 18). The *undulated extensive* (*un^{ex}*) allele carries a deletion that includes the last exon of the *Pax1* gene (19). In spite of lacking the last exon, mutant *Pax1* mRNA can be detected by RNase protection assay (19). In the *Undulated short-tail* (*Un^s*) allele, the complete *Pax1* locus is deleted (11, 17). In the following, we will refer to *un*, *un^{ex}*, and *Un^s*, as *Pax1^{un}*, *Pax1$^{un\text{-}ex}$*, and *Pax1$^{Un\text{-}s}$*, respectively.

The phenotypes of the classical *undulated* alleles have already been analyzed in detail (10–12, 19–21). In general, in all three alleles the vertebral column (10), the pectoral girdle (12), the sternum (19), and the thymus (11) are affected by size reductions and/or malformations. However, phenotypic differences can be observed among the *undulated* alleles. The *Pax1^{un}* and *Pax1$^{un\text{-}ex}$* mutations are regarded to be recessive because severe skeletal malformations are found only in homozygous animals (17). Nevertheless, occasional mild skeletal abnormalities have been described in heterozygotes of both alleles (10, 19, 20). In contrast, the *Pax1$^{Un\text{-}s}$* mutation is semidominant as heterozygotes exhibit clear skeletal abnormalities including a very short and strongly kinked tail (10). Homozygous *Pax1$^{Un\text{-}s}$* mice die perinatally displaying the most severe skeletal malformations among the *undulated* alleles. As the entire *Pax1* locus is absent in the semidominant *Pax1$^{Un\text{-}s}$* mutation, it has been considered to be a null allele, whereas the *Pax1^{un}* and *Pax1$^{un\text{-}ex}$* alleles have been regarded to be hypomorphs with weaker phenotypes compared with that of *Pax1$^{Un\text{-}s}$*. Based mainly on both the semidominant phenotype and the loss of *Pax1* in the *Pax1$^{Un\text{-}s}$* mutation, *Pax1* has been discussed to be haploinsufficient. Nevertheless, a *Pax1* null phenotype caused solely by the complete loss of Pax1 function remains to be elucidated because it is not known whether the absence of the *Pax1* gene alone results in the phenotype of the *Pax1$^{Un\text{-}s}$* deletion mutant.

To create a defined null allele, we have inactivated the *Pax1* gene by gene targeting. To our surprise, we found considerable differences between the phenotypes of the *Pax1* knockout and the *Pax1$^{Un\text{-}s}$* mutant mice. This finding indicates the contribution of additional gene(s) to the *Pax1$^{Un\text{-}s}$* phenotype. Instead, we show that the *Pax1* null phenotype resembles that of the *Pax1^{un}* and *Pax1$^{un\text{-}ex}$* alleles. Moreover, based on our detailed analysis of the heterozygous knockout mice, we prove haploinsufficiency of *Pax1* in skeletal elements of the vertebral column and the sternum.

MATERIALS AND METHODS

Generation of *Pax1* Knockout Mice. A *Pax1* genomic clone was isolated from a 129/Ola genomic cosmid library, and a 5.3-kb genomic *Hin*dIII fragment of the 5′ region of *Pax1*, including exon 1 and 2, was subcloned into pBluescript (Stratagene), designated as pBPax1H. A 1.0-kb *Xba*I genomic fragment from pBPax1H located downstream of exon 2 was cloned into pTZ19R (Pharmacia Biotech), generating the short arm of the targeting vector. In the next step, a 1.6-kb *Hin*dIII-*Pst*I fragment followed by the 3′ adjacent 1.2-kb *Pst*I fragment were inserted to generate the long arm of the targeting vector. The 1.6-kb *Sal*I-*Xho*I PGKneo cassette was inserted in opposite

The publication costs of this article were defrayed in part by page charge payment. This article must therefore be hereby marked "*advertisement*" in accordance with 18 U.S.C. §1734 solely to indicate this fact.

This paper was submitted directly (Track II) to the *Proceedings* office.
Abbreviations: *Un^s*, *Undulated short-tail*; *un^{ex}*, *undulated extensive*; *un*, *undulated*; E, embryonic day; ES cells, embryonic stem cells.

*Present address: metaGen, Gesellschaft für Genomforschung mbH, 14195 Berlin-Dahlem, Germany.
†To whom reprint requests should be addressed. e-mail: imai@gsf.de.

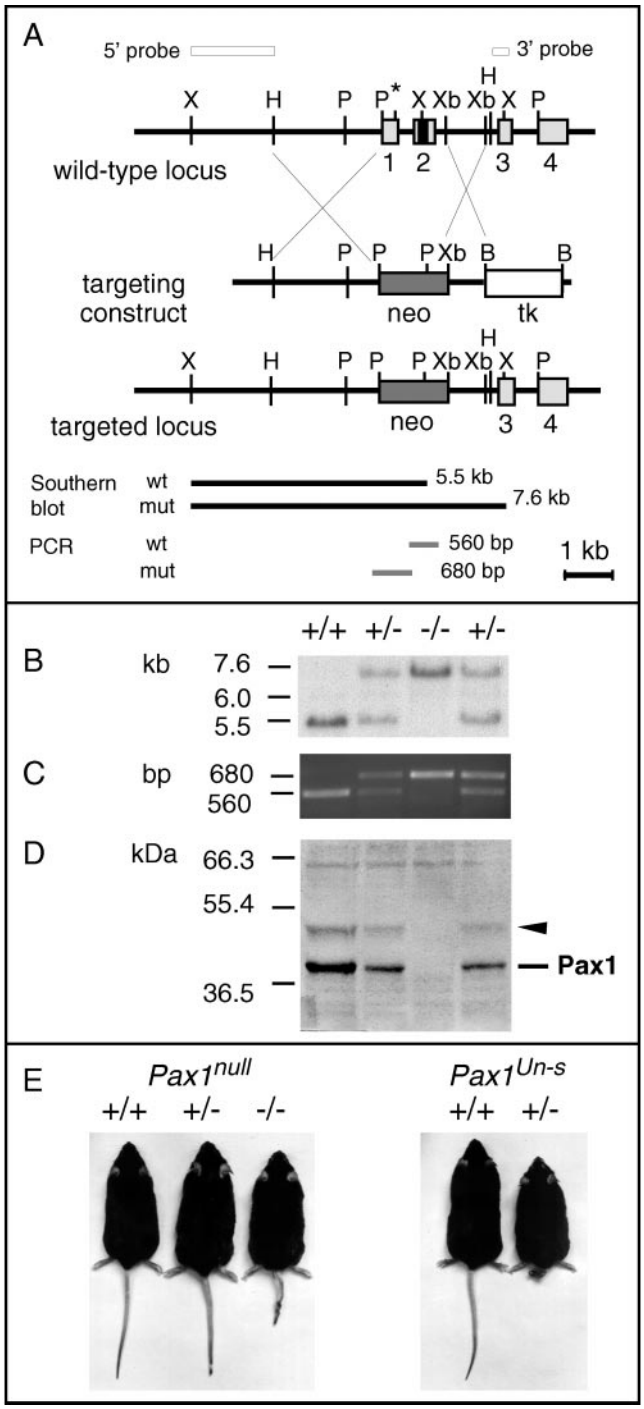

FIG. 1. Targeted disruption of the mouse *Pax1* gene. (*A*) Genomic structure of the *Pax1* locus and the targeting construct. Light gray colored boxes represent exons 1–4, whereas the black box in exon 2 represents the paired box. The 5′ and 3′ external probes used for the detection of the targeted allele in the Southern blot analysis are shown as open bars. Black bars indicate the fragments detected by Southern blot analysis with the 5′ probe, whereas grey bars indicate the PCR fragments. B, *Bam*HI; H, *Hin*dIII; P, *Pst*I; Xb, *Xba*I; X, *Xho*I; ∗, start point of translation; tk, MC1-HSV-tk; neo, PGK-neo. (*B*) Southern blot analysis of genomic DNA from wild-type (+/+), heterozygous (+/−), and homozygous (−/−) *Pax1* knockout mice. Liver DNA (10 μg) digested with *Xho*I was hybridized with the 5′ probe (see *A*). (*C*) Genotyping by PCR. The amplification products of the wild-type and mutated allele are depicted in *A*. (*D*) Western blot analysis of vertebral column protein extracts from E13.5 embryos. Two bands, the Pax1 protein at 42 kDa and an additional band at 50 kDa (arrowhead), are detected in heterozygous and wild-type control, but not in homozygous protein extracts. (*E*) *Pax1*^{null} mice, 9 months old (wild-type control, heterozygous, and homozygous littermates, left to right), and *Pax1*$^{Un\text{-}s}$ mice, 8 months old (wild-type control and heterozygous littermate, left to right). The tail-tip of the *Pax1*^{null} heterozygous mouse has been clipped.

orientation to that of the *Pax1* gene. Finally the 1.8-kb *Bam*HI MC1-HSV-tk cassette was cloned into the targeting vector, now called pPax1tg2. The vector was linearized by *Sca*I, and 20 μg of the construct were electroporated into 1.6×10^7 R1 embryonic stem (ES) cells (22) at 250 V and 0.5 mF by using a Gene Pulser (Bio-Rad). Stable clones were grown under double selection by using 200 μg/ml G418 and 2 μM gancyclovir in ES cell medium (23). Stable cell lines were tested for homologous recombination by Southern blot analysis by using a 5′ and a 3′ external probe. ES cells from correctly targeted clones were aggregated to morulae derived from CD1 donor mice and implanted into pseudopregnant CD1 female mice. Chimeric males were mated to C57BL/6 females and the offspring was genotyped by Southern blot and PCR analysis. PCR analysis was performed by using two sets of primer pairs in a single reaction (5′-CTCGCCTGCTCACTCCTATCCG-3′, forward primer, and 5′-ATGAGTGCCCATCTTAGTGC-3′, reverse primer of the wild-type *Pax1* allele, and 5′-CGTGACTGTAGAGATTGACG-3′, forward primer, and 5′-TGTCGATCAGGATGATCTGG-3′, reverse primer of the targeted *Pax1* allele) at 94°C for 1 min, 60°C for 1 min, and 72°C for 1 min in 32 cycles. Homozygous animals were generated by matings between heterozygotes, and newborn animals from generations two to three were used for this study.

Western Blot Analysis. E13.5 embryos from heterozygote intercrosses were dissected by cutting off the head and the limbs and removing all internal organs. The remainder was trimmed for most optimal enrichment of vertebral column tissue, and protein extracts were generated. Yolk sac material was collected for DNA preparation and subsequent genotyping by PCR. The protein extracts (30 μg) were subjected to Western blot analysis by using reducing SDS/PAGE conditions, as described (24). A Pax1-specific antiserum was generated by conjugating a 15-aa peptide from the C-terminal part of the Pax1 protein (amino acids 327–341; FKHREGTDRK-PPSPG) to keyhole limpet hemocyanin (KLH; Pierce). Two rabbits were immunized s.c. each with 400 μg of the KLH-conjugated Pax1-peptide in Freund's adjuvant. Subsequently, by using 100 μg of the fusion protein in Freund's adjuvant, the rabbits were boosted in 4-week intervals. The fourth immune serum of one rabbit, designated as 288-IV, was used with 1:250 dilution.

Animals. The *undulated* mice were purchased from The Jackson Laboratory. *Undulated extensive* and *Undulated short tail* mice were kindly provided by J. L. Cruickshank (Leeds, U.K.) and A. M. Malashenko (Krosnogorsk, Russia), respectively. Mice from the three *undulated* alleles have been crossed with C57BL/6 mice for more than 12 generations to establish congenic lines.

Skeletal Preparations. For skeletal preparations we used newborns heterozygous and homozygous for the targeted allele and wild-type littermates that were obtained from heterozygous intercrosses. The newborns were dissected and skeletons were stained with alcian blue for cartilage and alizarin red for bone as described (25).

RESULTS

Generation of a *Pax1* Null Mutation. For the purpose of generating a defined *Pax1* null mutation, the murine *Pax1* gene was disrupted by gene targeting. The targeting strategy was designed to delete the first two coding exons of *Pax1* (Fig. 1*A*). Exon 1 harbors the translational start codon, and exon 2 contains the entire paired box of the *Pax1* gene. From 300

stable ES cell clones tested, five proved to be correctly targeted. Male chimeras were generated by morula aggregation from two correctly targeted ES cell lines. Chimeras from one ES cell line passed the mutated allele to the offspring. In these mice, the expected targeting event was confirmed by Southern blot and PCR analyses (Figs. 1 *B* and *C*).

To prove the absence of Pax1 protein in the mutated mouse line, Western blot analysis was performed. We have generated a polyclonal antiserum directed against the C-terminal part of the Pax1 protein, designated as 288-IV. The Pax1 specificity of this antiserum was demonstrated in Western blot analyses by using protein extracts from $Pax1^{Un\text{-}s}$ mutant as well as wild-type control embryos. A 42-kDa band representing the Pax1 protein was detected in wild-type embryos, but was absent in homozygous $Pax1^{Un\text{-}s}$ embryos (data not shown). In embryos homozygous for the targeted allele Pax1 protein was not detectable, whereas it appeared at a reduced level in heterozygotes compared with wild-type controls (Fig. 1*D*). We therefore regard the targeted allele to be a defined null mutation of *Pax1*, designated as $Pax1^{null}$. Interestingly, in addition to the authentic Pax1 protein, antiserum 288-IV detected a protein at approximately 50 kDa that was also found to be reduced in heterozygotes and absent in homozygotes (arrowhead, Fig. 1*D*).

Mice of the expected genotypes from crosses between $Pax1^{null}$ heterozygotes are born at a Mendelian ratio (Table 1). A genetic complementation test between $Pax1^{null}$ and $Pax1^{un}$ mice confirmed allelism (not shown).

$Pax1^{null}$ heterozygous mice have an external appearance indistinguishable from that of wild-type littermates, whereas the homozygotes display a strongly kinked tail (Fig. 1*E*). Though smaller in size than heterozygous and wild-type mice, the $Pax1^{null}$ homozygotes are viable and fertile. Thus, from their appearance, they are similar to homozygous mice of the $Pax1^{un}$ and $Pax1^{un\text{-}ex}$ alleles (10), whereas they do not resemble $Pax1^{Un\text{-}s}$ mutant mice (Fig. 1*E*).

Skeletal Abnormalities in $Pax1^{null}$ Homozygous Mice. Examinations of skeletal preparations from homozygous $Pax1^{null}$ newborn animals showed strong skeletal abnormalities all along the vertebral column (Figs. 2 and 3*D*), in the sternum, and in the scapula (Fig. 2) with full penetrance (Table 1). In general, skeletal structures affected in $Pax1^{null}$ mutants are the same as those found in mutant mice of the three classical *undulated* alleles. In spite of these similarities, $Pax1^{null}$ mutants exhibit significant differences to both $Pax1^{un}$ and $Pax1^{Un\text{-}s}$ mutant mice with respect to the severity of the skeletal abnormalities (Fig. 3).

Axial Skeleton. In wild-type newborns, the ventral structure of the first cervical vertebra (C1, atlas), the *arcus anterior atlantis*, is separated from the odontoid process of the second cervical vertebra (C2, axis) by a distinct space (Fig. 2*A*). In homozygous newborns, this distinct space is not preserved as the odontoid process and the *arcus anterior atlantis* are fused by ventral cartilaginous and ossified bridges (Fig. 2*C*, arrow). The pedicles of C2 extend ventro-medially, and the ossified part of the arcus, the ventral tubercle, is enlarged (Fig. 2*C*, small arrowhead). In addition, in the cervical region ossification centers of the vertebral bodies are reduced or have not formed yet (Fig. 3*D*, yellow arrowhead). In the thoracic region the pedicles extend ventro-medially, resulting in fusions of the pedicles to the ossification centers of the vertebral bodies. These fusions start from around the fifth thoracic segment (T5) and extend toward the sacral and caudal segments (Fig. 3*D*). At the thoracic segments T11 to T13 the rib heads (*caput costae*) are ossified and fused to the pedicles, although a floating 13th rib can also be observed frequently (9/20; Fig. 3*D*, small arrowheads). Furthermore, the lower thoracic and lumbar vertebrae display an abnormal shape resulting from pronounced fusions of the pedicles across the ventral midline (Figs. 2*F* and 3*D*). In the lumbar region we observed saggitally split vertebrae predominantly in L3, L4, and/or L5 (Figs. 2*F* and 3*D*). In these segments, intervertebral discs are not formed; instead, a ventral cartilaginous rod-like structure is found (Fig. 2*F*, yellow arrowhead). Furthermore, the costal processes (Fig. 2*F*, small arrowhead) and the anapophyses are not formed (data not shown). These abnormalities in the lumbar region can consequently lead to skoliosis (Figs. 2*F* and 3*D*). In the tail, the not yet ossified caudal segments are triangular in shape which is caused by a strong reduction of the posterior halves of the vertebrae (Fig. 2*I*, *Inset*).

Sternum and Scapula. The sternum of wild-type newborns displays a regular pattern of ossified sternebrae and cartilaginous intersternebrae to which the ribs attach (Fig. 2*J*). In homozygous $Pax1^{null}$ newborns sternebrae 4 and 5 are fused, which is caused by complete ossification of the corresponding intersternebra (Fig. 2*L*, arrowhead). Only a restricted area next to the rib attachment site is chondrified. In few cases the ossification of the intersternebrae extends toward sternebra 3 (data not shown).

In the pectoral girdle the acromion, a chondrified process of the spine of the scapula connects to the humerus and to the clavicle (Fig. 2*M*). In homozygous $Pax1^{null}$ newborns the acromion process and a part of the spine are not formed (Fig. 2*O*). In all homozygotes examined both scapulae were always affected to the same extent.

Skeletal Abnormalities in $Pax1^{null}$ Heterozygous Mice. In 88% of the skeletons from heterozygous $Pax1^{null}$ newborns we observed skeletal abnormalities in the first two cervical vertebrae, in the lumbar region, and/or the sternum (overall ratio, Table 1). In contrast, the tail and the scapulae displayed no malformations in heterozygotes (Table 1; Fig. 2 *H* and *N*).

In the majority (63%) of the $Pax1^{null}$ heterozygous newborns, the axis (C2) is ventrally fused to the arcus of the atlas (C1) by cartilaginous bridges (Fig. 2*B*). These fusions are less pronounced than in homozygous littermates (Fig. 2C). In addition, the ventral tubercle of the arcus is enlarged (Fig. 2*B*, small arrowhead).

In nearly half (44%) of the heterozygous newborns we found abnormalities of vertebral elements in the lumbar region. In most cases the fourth lumbar vertebra (L4) displays a dual ossification center (Fig. 2*E*). As a rather rare consequence (3/32), the pedicles fuse to one of the twin ossification centers (Fig. 2*E*), and costal processes of the affected vertebrae are missing (data not shown).

One-third (34%) of the examined $Pax1^{null}$ heterozygous newborns exhibit a thin stripe of medio-saggital ossification of intersternebra 5 connecting sternebrae 4 and 5 (Fig. 2*K*). These sternebrae fusions are less severe than those found in homozygous littermates (Fig. 2*L*).

Table 1. Statistics of inheritance and of skeletal phenotypes in newborn animals from crosses between $Pax1^{null}$ heterozygotes

	+/+	+/−	−/−
Genotype			
Numbers	19	32	20
Ratio	0.27	0.45	0.28
Skeletal abnormalities, %			
Atlas-axis	10 (2)	63 (20)	100 (20)
Lumbar vertebrae	16 (3)	44 (14)	100 (20)
Tail	0 (0)	0 (0)	100 (20)
Sternum	5 (1)	34 (11)	100 (20)
Scapula	0 (0)	0 (0)	100 (20)
Overall	31 (6)	88 (28)	100 (20)

The percentage of animals with abnormalities in a given skeletal structure are listed in columns corresponding to their genotypes. The numbers of animals with abnormalities are given in parentheses. For the ratio of overall phenotype per genotype, the total number of animals with any of the described malformations was counted. For description of phenotypes, see text.

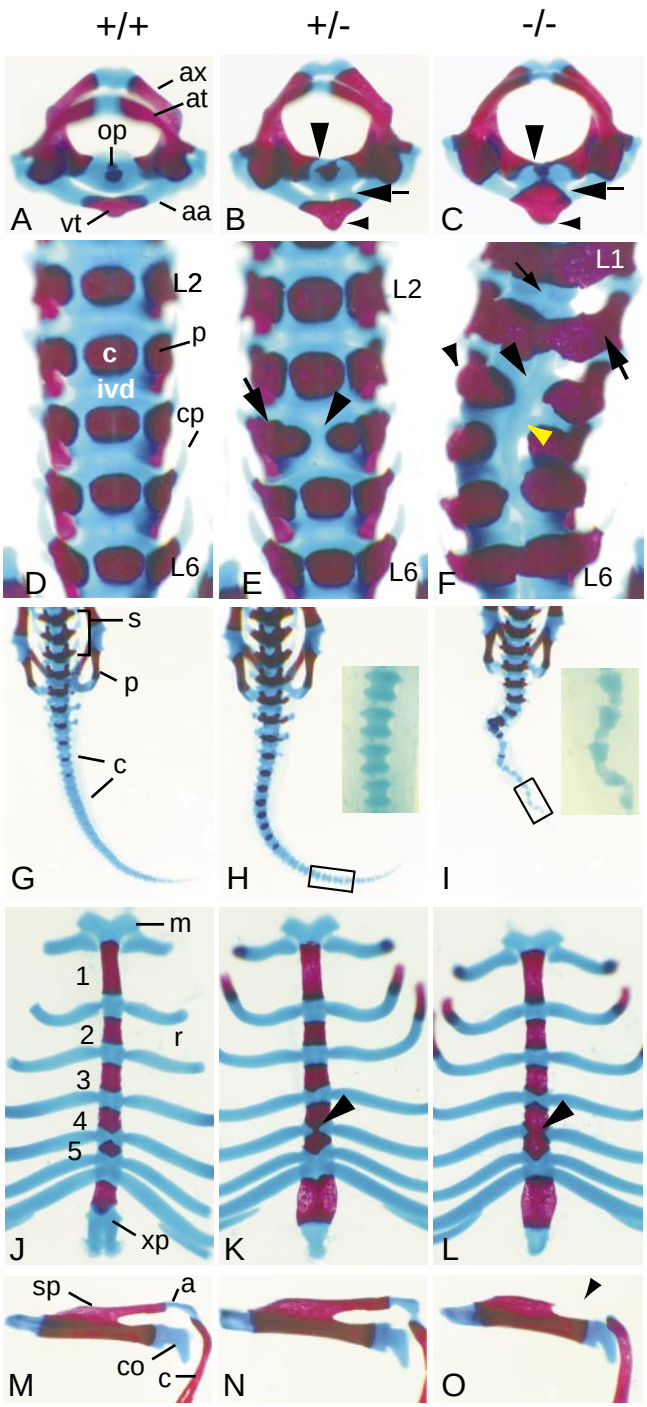

FIG. 2. Skeletal structures of wild-type (*A*, *D*, *G*, *J*, and *M*), heterozygous (*B*, *E*, *H*, *K*, and *N*), and homozygous (*C*, *F*, *I*, *L*, and *O*) *Pax1*^{null} newborn mice. (*A–C*) Superior view of atlas (at) and axis (ax). (*A*) Wild-type newborn. The odontoid process (op) of the axis is clearly separated from the arcus anterior atlantis (aa). vt, Ventral tubercle. (*B*) In heterozygous animals the ossified ventral tubercle is enlarged (small arrowhead) and is fused to the axis via cartilaginous bridges (arrow). Medial extensions of the pedicles of the axis are indicated by a large arrowhead. (*C*) In homozygous newborns the ossified ventral tubercle of the arcus anterior atlantis is enlarged (small arrowhead) and fused to the odontoid process of the axis (arrow). The pedicles of the axis extend medially to the ossification center of the vertebral body (large arrowhead). (*D–F*) Ventral view of lumbar vertebrae. (*D*) In wild-type newborns the ossification centers of the vertebral bodies (c) are clearly separated from the pedicles (p). Lumbar vertebrae L2 to L6 are shown, each separated by intervertebral discs (ivd). cp, Costal processes. (*E*) Lumbar vertebrae L2 to L6 of a heterozygous newborn with dual ossification center at L4 (arrowhead) are shown. The right part of the ossification center of L4 is fused to the right pedicle (arrow). (*F*) Lumbar vertebrae L1 to L6 of homozygous newborn. All lumbar vertebrae display fusions of the pedicles to the ossification centers (large arrow). In L3 to L5 vertebrae are saggitally split, ossification centers are missing (large arrowhead), and costal processes are lacking (small arrowhead). Intervertebral discs are reduced (small arrow), whereas in the sagittally split vertebrae a cartilaginous rod-like structure is formed medially (yellow arrowhead). Note that the malformations lead to skoliosis. (*G–I*) Dorsal views of sacrum and tail. (*G*) The sacral (s) and caudal (c) vertebrae of a wild-type newborn animal are shown; p, pelvic girdle. (*H*) In heterozygotes no difference to wild-type sacrum and tail can be observed. (*Inset*) A part of the tail (C16–19) in close-up. (*I*) Homozygous animals exhibit a strongly kinked tail. (*Inset*) The caudal segments C16–20 are shown in close-up. The vertebrae have a triangular shape caused by a drastically reduced posterior half of the segments. (*J–L*) Ventral view of the sternum. (*J*) In wild-type newborns the ossified sternebrae 1–5 are clearly separated by cartilaginous intersternebrae, to which the ribs attach. m, Manubrium; r, rib; xp, xiphoid process. (*K*) In heterozygotes the cartilaginous intersternebra between sternebrae 4 and 5 frequently exhibits a thin stripe of medio-sagittal ossification (arrowhead). (*L*) Homozygous newborns show complete ossification of the intersternebra connecting sternebrae 4 and 5 (arrowhead). (*M–O*) Left scapula in superior view. (*M*) Wild-type scapula connected to the clavicula (c) via the acromion (a); sp, spine of the scapula; co, coracoid process. (*N*) Scapula of heterozygote, indistinguishable from that of a wild-type newborn. (*O*) Scapula from homozygous newborn animal, displaying lack of a part of the ossified spine and of the cartilaginous acromion (arrowhead).

DISCUSSION

To get clear insight into a defined *Pax1* null phenotype and furthermore to clarify whether or not *Pax1* is haploinsufficient, we created a *Pax1* mutation by gene targeting. Our results show that this knockout allele represents a defined null mutation of *Pax1*.

Interestingly, the detection of a 50-kDa protein, in addition to the previously described 42-kDa Pax1 protein (18), indicates the presence of a second version of the Pax1 protein generated by some unknown mechanism. The reduction in amount of both the 50-kDa band and the 42-kDa band in *Pax1*^{null} heterozygotes, and the absence of both in *Pax1*^{null} homozygotes support this assumption.

***Pax1*^{null} and the Undulated Alleles.** To our surprise, both heterozygous and homozygous mutants of the *Pax1*^{null} allele do not resemble the corresponding *Pax1*$^{Un\text{-}s}$ mutant mice in their appearance (Fig. 1*E*; refs. 10, 17, and 19). As the *Pax1*^{null} heterozygotes are indistinguishable from wild-type littermates, and the *Pax1*^{null} homozygotes are viable, they are similar to mutant mice of the *Pax1*^{un} and *Pax1*^{null} alleles (10).

Furthermore, from our analysis of the skeletal phenotypes we conclude that *Pax1*^{null} homozygous mice resemble that of *Pax1*^{un} and *Pax1*$^{un\text{-}ex}$ homozygotes. Nevertheless, the *Pax1*^{un} phenotype is less severe than that of the *Pax1* null allele, suggesting *Pax1*^{un} to be a hypomorph (Fig. 3 *B* and *D*; refs. 10, 19, and 20). On the other hand, *Pax1*$^{un\text{-}ex}$ and *Pax1*^{null} mice exhibit virtually identical skeletal phenotypes (Fig. 3 *C* and *D*). Therefore we assume that in the *Pax1*$^{un\text{-}ex}$ allele no other gene(s) beside *Pax1* are involved in the resulting phenotype, and that *Pax1*$^{un\text{-}ex}$ may be a natural null allele. In contrast, the skeletal phenotype of *Pax1*$^{Un\text{-}s}$ homozygous newborns is much stronger than that of *Pax1*^{null} homozygotes (Fig. 3 *D* and *E*).

In the *Pax1*$^{Un\text{-}s}$ mutation the five coding exons of the *Pax1* gene, which are located within a region of 10 kb, are known to be deleted (2, 17). The obvious phenotypic differences we found between the *Pax1*^{null} and the *Pax1*$^{Un\text{-}s}$ allele suggest that not only *Pax1* but also additional gene(s) are involved in the *Pax1*$^{Un\text{-}s}$ mutation. The *Pax1*$^{Un\text{-}s}$ deletion, formerly described to cover at least 48.3 kb (19), is more than 100 kb in size (B.W. and K.I., unpublished observations). We consider the deletion to be large enough to harbor additional gene(s). Interestingly,

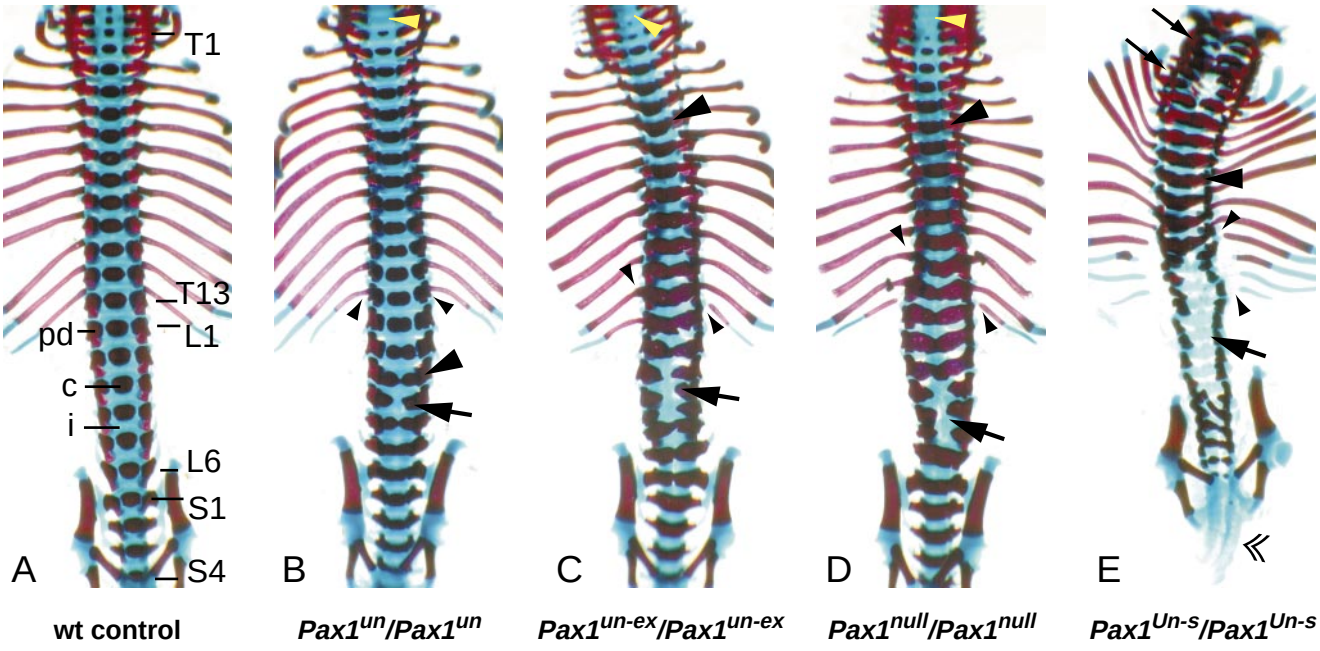

FIG. 3. Ventral view of vertebral columns of *Pax1*^{null} and the classical *undulated* homozygous mice at the newborn stage. (*A*) Wild-type newborn, displaying no phenotypic abnormalities. Vertebral elements from the sixth cervical (C6) to the last sacral (S4) segment are shown. T1–T13, thoracic vertebrae; L1–L6, lumbar vertebrae; S1–S4, sacral vertebrae; pd, pedicle; c, ossification center of vertebral body; i, intervertebral disc. (*B*) *Pax1*^{un} homozygote. The ossification center of C7 is missing (yellow arrowhead). Fusions of pedicles to ossification centers at L3 (large arrowhead) and all caudally following segments. Dual ossification centers are found from L2 to L5, and the completely split centrum of L4 is indicated by an arrow. Note that the proximal ends of the 13th rib pair are ossified (small arrowheads). (*C*) *Pax1*$^{un\text{-}ex}$ homozygote. The ossification center of C5 is missing, and of C6 and C7 are reduced (yellow arrowhead). Fusions of pedicles to ossification centers at T5 (large arrowhead) and all caudally following segments. Vertebrae of the lumbar region (L2 to L4) are saggitally split (arrow). The left 13th rib is not connected to its respective vertebra, and the rib heads of rib pair 12 and the single right rib 13 and left rib 11 are ossified (small arrowheads). (*D*) *Pax1*^{null} homozygote with no ossification centers in vertebrae C5 and C6 (yellow arrowhead). Note that pedicles fuse to ossification centers from T5 (large arrowhead) on caudally, and vertebrae of the lumbar region (L3 to L5) are sagittally split (arrow). Note that these malformations lead to skoliosis. The 13th rib pair is not connected to its respective vertebra, and the proximal ends of rib pairs 11 and 12 are ossified (small arrowheads). (*E*) *Pax1*$^{Un\text{-}s}$ homozygote. Intervertebral discs and vertebral bodies are missing or strongly malformed all along the vertebral column. In addition, in the cervical region vertebrae are ventrally split (small arrows), whereas thoracic vertebrae display fusions between pedicles and ossification centers (large arrowhead). In the lumbar region all ossification centers are missing (large arrow) and the tail is extremely shortened (double arrowhead). The lower ribs are not connected to the vertebral column (small arrowheads).

only *Pax1*-expressing tissues are affected in *Pax1*$^{Un\text{-}s}$ mutant mice (10). Therefore, we can make certain assumptions about the mechanism of how these additional gene(s) could contribute to the phenotype. For example, a second gene is codeleted which shares expression domains with *Pax1* during embryogenesis. Alternatively, as a result of the deletion, a gene located in regions flanking the deletion breakpoints comes under the influence of some distant, yet unknown *Pax1* regulatory elements. In this model the second gene could be ectopically activated that in combination with loss of *Pax1* would lead to a gain-of-function phenotype in *Pax1*$^{Un\text{-}s}$. Recently an example for this model has been reported for the *Patch* (*Ph*) mutation in which the complete *PDGFRα* gene is deleted. In *Ph*, a gene located outside the deletion, *c-kit*, was found to be ectopically expressed and assumed to contribute to the *Ph* gain-of-function phenotype (26).

Currently we are performing several approaches to elucidate the molecular basis of the *Pax1*$^{Un\text{-}s}$ mutation. We are in the process of physically mapping the *Pax1*$^{Un\text{-}s}$ deletion breakpoints and in parallel have started to search for genes located in the vicinity of *Pax1*. Furthermore, experiments to determine the promoter and regulatory elements of the *Pax1* gene are underway, as these could not be successfully identified to date. However, preliminary promoter studies suggest that a 3-kb genomic fragment, including the 2-kb region upstream of the first exon, is insufficient to direct specific spatio-temporal *Pax1* expression (S.-P. Yee and K.I., unpublished observations). For these purposes, we have established a bacterial artificial chromosome (BAC) contig surrounding the *Pax1* locus. By generating mice transgenic for BACs which contain the *Pax1* gene we have started rescue experiments for the *Pax1*^{null} and *Pax1*$^{Un\text{-}s}$ alleles.

***Pax1* Is Haploinsufficient.** Although *Pax1*^{null} heterozygous mice appear externally normal, we demonstrate in this study that almost 90% of the heterozygotes exhibit moderate skeletal malformations in the sternum and parts of the vertebral column. This finding indicates that the *Pax1*^{null} mutation is semidominant, thus proving haploinsufficiency of *Pax1*. In contrast, the scapula and the tail are normal in all heterozygotes, showing recessiveness of *Pax1*^{null} in these structures.

Previous studies on the skeletal phenotypes of *Pax1*^{un} and *Pax1*$^{un\text{-}ex}$ mutant mice showed weak abnormalities in the sternum and in parts of the vertebral column of heterozygotes (10, 19, 20). Nevertheless, a null phenotype caused solely by the complete loss of Pax1 function could not be defined, and thus haploinsufficiency of *Pax1* could not be concluded from these observations.

As not all heterozygous animals are affected to the same extent, the penetrance of the *Pax1*^{null} heterozygous phenotype seems to be influenced by genetic background effects. On the other hand, the homozygous phenotype shows full penetrance, and the range of variation in phenotypic severity among the homozygotes is much smaller than that among heterozygotes. For comparison, we also have carefully examined wild-type littermates. Less frequently than in heterozygotes, we indeed found recognizable skeletal abnormalities in wild-type controls that, however, in all cases were milder than those observed in heterozygotes.

We could demonstrate that in the developing vertebral column of *Pax1*^{null} heterozygotes the level of Pax1 protein is reduced. This result, together with the observation of skeletal abnormalities in *Pax1*^{null} heterozygotes, suggests that Pax1 dosage is critical for the formation of ventral vertebral elements of the cervical and lumbar region, and the sternum.

The *Pax1* null mutant described in this report will be an important tool to study genetic interactions between *Pax1* and other genes. One of these genes is *Pax9* which is highly related to *Pax1*. Both genes belong to the same subfamily of *Pax* genes (2, 27) and have a similar sequence, gene structure, and expression pattern (28). Therefore, it is possible that *Pax9* might partially substitute for *Pax1*. The *Pax9* gene has recently been inactivated by gene targeting (29). To investigate a potential redundancy between these genes, we are in the process of analyzing double mutants between *Pax1* and *Pax9* null mice.

We thank Drs. M. Hrabé de Angelis, T. Wilm and S.-P. Yee for discussion of the manuscript. We are grateful to U. Huffstadt and S. Bourier for excellent technical assistance with the gene targeting experiment, and U. Linzner (Institute for Pathology/GSF) for the generation of the oligonucleotide primers. This work was in part supported by the Deutsche Forschungsgemeinschaft.

1. Walther, C., Guenet, J.-L., Simon, D., Deutsch, U., Jostes, B., Goulding, M. D., Plachov, D., Balling, R. & Gruss, P. (1991) *Genomics* **11,** 424–434.
2. Wallin J., Mizutami, Y., Imai, K., Miyashita, N., Moriwaki, K., Taniguchi, M., Koseki, H. & Balling, R. (1993) *Mamm. Genome* **4,** 354–358.
3. Bopp, D., Burri, M., Baumgartner, S., Frigerio, G. & Noll, M. (1986) *Cell* **47,** 1033–1040.
4. Treisman, J., Harris, E. & Desplan, C. (1991) *Genes Dev.* **5,** 594–604.
5. Miskiewicz, P., Morrisey, D., Lan, Y., Raj, L., Kessler, S., Fujioka, M., Goto, T. & Weir, M. (1996) *Development (Cambridge, U.K.)* **122,** 2709–2718.
6. Brand, M., Heisenberg, C. P., Jiang, Y. J., Beuchle, D., Lun, K., Furutani-Seiki, M., Granato, M., Haffter, P., Hammerschmidt, M., Kane, D. A., *et al.* (1996) *Development (Cambridge, U.K.)* **123,** 179–190.
7. Fu. W. & Noll, M. (1997) *Genes Dev.* **11,** 2066–2078.
8. Dahl, E., Koseki, H. & Balling, R. (1997) *BioEssays* **19,** 755–765.
9. Deutsch, U., Dressler, G. R. & Gruss, P. (1988) *Cell* **53,** 617–625.
10. Wallin J., Wilting, J., Koseki, H., Fritsch, R., Christ, B. & Balling, R. (1994) *Development (Cambridge, U.K.)* **120,** 1109–1121.
11. Wallin, J., Eibel, H., Neubüser, A., Wilting, J., Koseki, H. & Balling, R. (1996) *Development (Cambridge, U.K.)* **122,** 23–30.
12. Timmons, P. M., Wallin, J., Rigby, P. W. J. & Balling, R. (1994) *Development (Cambridge, U.K.)* **120,** 2773–2785.
13. Wright, M. E. (1947) *Heredity* **1,** 137–141.
14. Blandova, Z. K. & Egorov, I. K. (1975) *Mouse News Lett.* **52,** 43.
15. Wallace, M. E. (1985) *J. Hered.* **76,** 271–278.
16. Balling, R., Deutsch, U. & Gruss, P. (1988) *Cell* **55,** 531–535.
17. Balling, R., Lau, C. F., Dietrich, S., Wallin, J. & Gruss, P. (1992) *Postimplantation Development in the Mouse* (Wiley, Chichester, U.K.), pp. 132–143.
18. Chalepakis, G., Fritsch, R., Fickenscher, H., Deutsch, U., Goulding, M. & Gruss, P. (1991) *Cell* **66,** 873–884.
19. Dietrich, S. & Gruss, P. (1995) *Dev. Biol.* **167,** 529–548.
20. Grüneberg, H. (1950) *J. Genet.* **50,** 142–173.
21. Grüneberg, H. (1954) *J. Genet.* **52,** 441–455.
22. Nagy, A., Rossant, J., Nagy, R., Abramow-Newerly, W. & Roder, J. C. (1993) *Proc. Natl. Acad. Sci. USA* **90,** 8424–8428.
23. Wurst, W. & Joyner, A. L. (1993) in *Gene Targeting: A Practical Approach*, ed. Joyner, A. L. (Oxford Univ. Press, New York), pp. 33–61.
24. Peters, H., Doll, U. & Niessing, J. (1995) *Dev. Dyn.* **203,** 1–16.
25. Kessel, M., Balling, R. & Gruss, P. (1990) *Cell* **61,** 301–308.
26. Wehrle-Haller, B., Morrison-Graham, K. & Weston, J. A. (1996) *Dev. Biol.* **177,** 463–474.
27. Stapleton, P., Weith, A., Urbanek, P., Kozmik, Z. & Busslinger, M. (1993) *Nat. Genet.* **3,** 292–298.
28. Neubüser, A., Koseki, H. & Balling, R. (1995) *Dev. Biol.* **170,** 701–716.
29. Peters, H., Neubüser, A., Kratochwil, K. & Balling, R. (1998) *Genes Dev.*, in press.